Pumping velocity in homogeneous helical turbulence with shear

Igor Rogachevskii,[1,*] Nathan Kleeorin,[1,†] Petri J. Käpylä,[2,3,‡] and Axel Brandenburg[3,4,§]

[1]*Department of Mechanical Engineering, Ben-Gurion University of the Negev, P.O. Box 653, Beer-Sheva 84105, Israel*
[2]*Department of Physics, Gustaf Hällströmin katu 2a (P.O. Box 64), University of Helsinki, FI-00064 Finland*
[3]*NORDITA, AlbaNova University Center, Roslagstullsbacken 23, SE-10691 Stockholm, Sweden*
[4]*Department of Astronomy, Stockholm University, SE 10691 Stockholm, Sweden*

Using different analytical methods (the quasilinear approach, the path-integral technique, and the tau-relaxation approximation) we develop a comprehensive mean-field theory for a pumping effect of the mean magnetic field in homogeneous nonrotating helical turbulence with imposed large-scale shear. The effective pumping velocity is proportional to the product of α effect and large-scale vorticity associated with the shear, and causes a separation of the toroidal and poloidal components of the mean magnetic field along the direction of the mean vorticity. We also perform direct numerical simulations of sheared turbulence in different ranges of hydrodynamic and magnetic Reynolds numbers and use a kinematic test-field method to determine the effective pumping velocity. The results of the numerical simulations are in agreement with the theoretical predictions.

PACS number(s): 47.65.−d

I. INTRODUCTION

The origin of cosmic magnetic fields is one of the fundamental problems in theoretical physics and astrophysics. It is generally believed that solar and galactic magnetic fields are caused by the combined action of helical turbulent motions of fluid and differential rotation [1–7]. In most of these studies, differential rotation plays merely the role of enhancing the magnetic field in the toroidal direction. However, in recent years there has been increased interest in mean-field effects caused specifically by turbulent shear flows. This interest is caused by discoveries of the shear dynamo [8,9] and vorticity dynamo [10,11] in nonhelical homogeneous turbulence with a large-scale shear. In particular, recent numerical experiments [12–17] have clearly demonstrated the existence of a shear dynamo of a large-scale magnetic field in nonhelical turbulence or turbulent convection with superimposed large-scale shear. However, the origin of the shear dynamo is still subject of active discussions [8,9,15,18–23].

There are three additional phenomena that are also related to the presence of shear. One is the vorticity dynamo, which is the self-excitation of large-scale vorticity in a turbulence with large-scale shear. It has been predicted theoretically [10,11] and detected in recent numerical experiments [13,14,24]. The vorticity dynamo can also affect the dynamo process of the mean magnetic field. Another phenomenon is a nonzero α effect in nonhelical turbulence with shear when the system is inhomogeneous or density stratified. In that case there is an α effect [8,18] that can lead to an alpha-shear dynamo. Finally, when homogeneous turbulence with shear is helical, there is an effective pumping velocity $\boldsymbol{\gamma} \propto \alpha \boldsymbol{W}$ of the large-scale magnetic field, where $\boldsymbol{W}$ is the large-scale vorticity caused by shear. This effect has so far only been found in direct numerical simulations (DNS) [25], but there has so far been no theory

for this new effect, nor has there been a systematic survey of DNS for determining the dependence of pumping on magnetic Reynolds and Prandtl numbers as well as the turbulent Mach number.

The goal of the present study is to develop a comprehensive theory of mean-field pumping in homogeneous helical turbulence with shear and to perform systematic numerical simulations designed for detailed comparison with the theoretical predictions. It is important to emphasize that the pumping of the large-scale magnetic field discussed usually in the literature has always been connected with inhomogeneous turbulence [3,26,27], but here we study the pumping for homogeneous, albeit helical turbulence.

II. GOVERNING EQUATIONS

We consider homogeneous helical turbulence with a linear shear velocity $\overline{U} = (0,Sx,0)$. Averaging the induction equation over an ensemble of turbulent velocity field yields the mean-field equation:

$$\frac{\partial \overline{\boldsymbol{B}}}{\partial t} = \nabla \times (\overline{U} \times \overline{\boldsymbol{B}} + \overline{\boldsymbol{u} \times \boldsymbol{b}} - \eta \nabla \times \overline{\boldsymbol{B}}), \qquad (1)$$

where $\mathcal{E}_i \equiv (\overline{\boldsymbol{u} \times \boldsymbol{b}})_i = a_{ij}\overline{B}_j + b_{ijk}\nabla_k \overline{B}_j$ is the mean electromotive force, $\boldsymbol{u}$ and $\boldsymbol{b}$ are the fluctuations of velocity and magnetic field, overbars denote averaging over an ensemble of turbulent velocity fields, $\overline{\boldsymbol{B}}$ is the mean magnetic field, $\overline{U}$ is the mean velocity that includes only the imposed large-scale shear, and η is the magnetic diffusion due to electrical conductivity of the fluid. Note that the part $a_{ij}\overline{B}_j$ in the expression for the mean electromotive force determines the effective pumping velocity, $\gamma_i = -\frac{1}{2}\epsilon_{ijk}a_{ij}$, and the α tensor, $\alpha_{ij} = \frac{1}{2}(a_{ij} + a_{ji})$, i.e., $\mathcal{E}_i^{(a)} = \alpha_{ij}\overline{B}_j + (\boldsymbol{\gamma} \times \overline{\boldsymbol{B}})_i$, while the turbulent magnetic diffusion and the shear-current dynamo effect are associated with the b_{ijk} term.

To determine the turbulent transport coefficients in homogeneous helical turbulence with mean velocity shear we use the

*gary@bgu.ac.il
†nat@bgu.ac.il
‡petri.kapyla@helsinki.fi
§brandenb@nordita.org

following equations for fluctuations of velocity and magnetic field:

$$\frac{\partial \boldsymbol{u}}{\partial t} = -(\overline{\boldsymbol{U}}\cdot\nabla)\boldsymbol{u} - (\boldsymbol{u}\cdot\nabla)\overline{\boldsymbol{U}} - \frac{1}{\overline{\rho}}\nabla p + \frac{1}{4\pi\overline{\rho}}[(\boldsymbol{b}\cdot\nabla)\overline{\boldsymbol{B}}$$
$$+ (\overline{\boldsymbol{B}}\cdot\nabla)\boldsymbol{b}] + \nu\Delta\boldsymbol{u} + \boldsymbol{u}^N + \boldsymbol{f}^{(u)}, \tag{2}$$

$$\frac{\partial \boldsymbol{b}}{\partial t} = (\overline{\boldsymbol{B}}\cdot\nabla)\boldsymbol{u} - (\boldsymbol{u}\cdot\nabla)\overline{\boldsymbol{B}} + (\boldsymbol{b}\cdot\nabla)\overline{\boldsymbol{U}} - (\overline{\boldsymbol{U}}\cdot\nabla)\boldsymbol{b}$$
$$+ \eta\,\Delta\boldsymbol{b} + \boldsymbol{b}^N, \tag{3}$$

where ν is the kinematic viscosity, $\overline{\rho}$ is the mean density of the incompressible fluid flow, p is the fluctuation of total (hydrodynamic and magnetic) pressure, the magnetic permeability of the fluid is included in the definition of the magnetic field, $\boldsymbol{v}^N$ and $\boldsymbol{b}^N$ are the nonlinear terms, and $\overline{\rho}\,\boldsymbol{f}^{(u)}$ is the stirring force for the background velocity fluctuations.

We begin by deriving expressions for the pumping effect that are valid in different regimes, where fluid and magnetic Reynolds numbers are both small, both are large, or only the fluid Reynolds number is large, but the magnetic Reynolds number is small. These results will then be compared with those of DNS in the corresponding regimes.

A. Small magnetic and hydrodynamic Reynolds numbers

We use the quasilinear or second-order correlation approximation (SOCA) applied to shear flow turbulence (see [18,20]). This approach is valid for small magnetic and hydrodynamic Reynolds numbers. To exclude the pressure term from the equation of motion (2) we calculate $\nabla\times(\nabla\times\boldsymbol{u})$, then we rewrite the obtained equation and Eq. (3) in Fourier space, apply the two-scale approach (i.e., we use large-scale and small-scale variables), neglect nonlinear terms in Eqs. (2)–(3), but retain molecular dissipative terms in these equations. We seek a solution for fluctuations of velocity and magnetic fields as an expansion for weak velocity shear:

$$\boldsymbol{u} = \boldsymbol{u}^{(0)} + \boldsymbol{u}^{(1)} + \cdots, \tag{4}$$
$$\boldsymbol{b} = \boldsymbol{b}^{(0)} + \boldsymbol{b}^{(1)} + \cdots, \tag{5}$$

where

$$b_i^{(0)}(\boldsymbol{k},\omega) = G_\eta(k,\omega)\Big[i(\boldsymbol{k}\cdot\overline{\boldsymbol{B}})\delta_{ij} - \Big(\delta_{ij}\,k_m\frac{\partial}{\partial k_n}$$
$$+ \delta_{im}\delta_{jn}\Big)(\nabla_n\overline{B}_m)\Big]u_j^{(0)}(\boldsymbol{k},\omega), \tag{6}$$

$$u_i^{(1)}(\boldsymbol{k},\omega) = G_\nu(k,\omega)\Big(2k_{iq}\delta_{jp} + \delta_{ij}\,k_q\frac{\partial}{\partial k_p} - \delta_{iq}\delta_{jp}\Big)$$
$$\times (\nabla_p\overline{U}_q)\,u_j^{(0)}(\boldsymbol{k},\omega), \tag{7}$$

$$b_i^{(1)}(\boldsymbol{k},\omega) = G_\eta(k,\omega)\bigg\{\Big[i(\boldsymbol{k}\cdot\overline{\boldsymbol{B}})\delta_{ij} - \Big(\delta_{ij}\,k_m\frac{\partial}{\partial k_n}$$
$$+ \delta_{im}\delta_{jn}\Big)(\nabla_n\overline{B}_m)\Big]u_j^{(1)}(\boldsymbol{k},\omega) + \Big[\delta_{ij}\,k_q\frac{\partial}{\partial k_p}$$
$$+ \delta_{iq}\delta_{jp}\Big]b_j^{(0)}(\boldsymbol{k},\omega)\,(\nabla_p\overline{U}_q)\bigg\}. \tag{8}$$

Here $G_\nu(k,\omega) = (\nu k^2 - i\omega)^{-1}$, $G_\eta(k,\omega) = (\eta k^2 - i\omega)^{-1}$, and δ_{ij} is the Kronecker tensor. The statistical properties of the background velocity fluctuations with a zero large-scale shear,

$\boldsymbol{u}^{(0)}$, are assumed to be given. For derivation of Eqs. (6)–(8) we use the identity

$$\int \overline{U}_q(\boldsymbol{Q})\,b_n(\boldsymbol{k}-\boldsymbol{Q})\,d\boldsymbol{Q} = i(\nabla_p\overline{U}_q)\frac{\partial b_n}{\partial k_p},$$

which is valid in the framework of the mean-field approach; i.e., it is assumed that there is scale separation. Equations (6)–(8) coincide with those derived by [18], and they allow us to determine the cross-helicity tensor $g_{ij}^{(1)} = \langle u_i^{(0)} b_j^{(1)}\rangle + \langle u_i^{(1)} b_j^{(0)}\rangle$. This procedure yields the contributions $\mathcal{E}_m^{(S)} = \varepsilon_{mij}\int g_{ij}^{(1)}(\boldsymbol{k},\omega)\,d\boldsymbol{k}\,d\omega$ to the mean electromotive force caused by sheared helical turbulence. We are interested first of all in the contributions to the mean electromotive force which are proportional to the mean magnetic field, i.e., $\mathcal{E}_i^{(a)} = \alpha_{ij}\overline{B}_j + (\boldsymbol{\gamma}\times\overline{\boldsymbol{B}})_i$. For the integration in ω space and in $\boldsymbol{k}$ space we have to specify a model for the background shear-free helical turbulence (with $\overline{\boldsymbol{B}} = 0$), which is determined by the equation

$$\langle u_i(\boldsymbol{k},\omega)\,u_j(-\boldsymbol{k},-\omega)\rangle^{(0)}$$
$$= \frac{E(k)\,\Phi(\omega)}{8\pi\,k^2}\bigg[\Big(\delta_{ij} - \frac{k_i\,k_j}{k^2}\Big)\langle\boldsymbol{u}^2\rangle^{(0)}$$
$$- \frac{i}{k^2}\,\varepsilon_{ijl}\,k_l\,\langle\boldsymbol{u}\cdot(\nabla\times\boldsymbol{u})\rangle^{(0)}\bigg], \tag{9}$$

where $E(k)$ is the energy spectrum [e.g., a power-law spectrum, $E(k)\propto(k/k_{\rm f})^{-q}$ with the exponent $1 < q < 3$ for the wave numbers $k_{\rm f}\leqslant k\leqslant k_{\rm d}$, where $k_{\rm f}$ and $k_{\rm d}$ are the forcing and dissipation wave numbers], and ε_{ijk} is the fully antisymmetric Levi-Cività tensor. We consider the frequency function $\Phi(\omega)$ in the form of the Lorentz profile: $\Phi(\omega) = \nu k^2/[\pi\,(\omega^2 + \nu^2 k^4)]$. This model for the frequency function corresponds to the correlation function

$$\langle u_i(t)u_j(t+\tau)\rangle \propto \exp(-\tau\,\nu k^2). \tag{10}$$

In that case, and under the assumption of small magnetic and hydrodynamic Reynolds numbers, the effective pumping velocity $\boldsymbol{\gamma}$ and the off-diagonal components of the tensor α_{ij} are given by

$$\boldsymbol{\gamma} = \frac{C_1(q)}{2}\left(\frac{\rm Pm}{1+{\rm Pm}}\right)^2 {\rm Re}^2\,\tau_{\rm f}\,\alpha_*\,\overline{\boldsymbol{W}}, \tag{11}$$

$$\alpha_{ij} = \frac{C_1(q)}{5}\frac{(2{\rm Pm}+1)\,{\rm Pm}}{(1+{\rm Pm})^2}\,{\rm Re}^2\,\tau_{\rm f}\,\alpha_*\,(\partial\overline{U})_{ij}, \tag{12}$$

$$C_1(q) = \int_{k_{\rm f}}^{k_{\rm d}} E(k)\left(\frac{k}{k_{\rm f}}\right)^{-4} dk$$
$$= \left(\frac{q-1}{q+3}\right)\left[\frac{1-(k_{\rm f}/k_{\rm d})^{q+3}}{1-(k_{\rm f}/k_{\rm d})^{q-1}}\right], \tag{13}$$

where $\alpha_* = -(\tau_{\rm f}/3)\,\langle\boldsymbol{u}\cdot(\nabla\times\boldsymbol{u})\rangle^{(0)}$, ${\rm Pm} = \nu/\eta$ is the magnetic Prandtl number, ${\rm Re} = \tau_{\rm f}\,\langle\boldsymbol{u}^2\rangle^{(0)}/\nu$ is the hydrodynamic Reynolds number, ${\rm Rm} = {\rm Re}\,{\rm Pm}$ is the magnetic Reynolds number, and $\tau_{\rm f} = \ell_{\rm f}/u_{\rm rms}$ is the turnover time, where $\ell_{\rm f} = 1/k_{\rm f}$ is the energy-containing (forcing) scale of a random velocity field and $u_{\rm rms} = \sqrt{\langle\boldsymbol{u}^2\rangle^{(0)}}$. For the integration in ω space we use the integrals $I_n(k)$ given in Appendix A. For linear shear velocity, $\overline{U} = (0, Sx, 0)$, the mean vorticity is $\overline{\boldsymbol{W}} = \nabla\times\overline{U} = (0, 0, S)$, and the mean symmetric
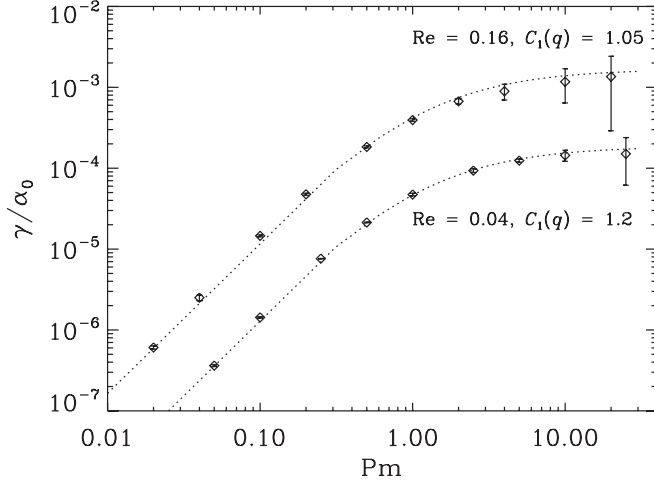
FIG. 1. Pumping coefficient $\gamma = \frac{1}{2}(a_{21} - a_{12})$ normalized by $\alpha_0 = \frac{1}{3} u_{\rm rms}$ as a function of Pm for two values of Re (Sets A1 and A2). The shear parameter Sh $= -0.20 \, (-0.13)$ for Re $= 0.04 \, (0.16)$. Analytical results according to Eq. (14) are overplotted with dotted lines. The values of $C_1(q)$ are used as fit parameters and indicated in the legends.

tensor $(\partial \overline{U})_{ij} = (\nabla_i \overline{U}_j + \nabla_j \overline{U}_i)/2$ has only two nonzero components: $(\partial \overline{U})_{12} = (\partial \overline{U})_{21} = S/2$. Therefore, α_{ij} has two nonzero off-diagonal components caused by both shear and helical turbulence $\alpha_{12} = \alpha_{21}$, while the effective pumping velocity $\boldsymbol{\gamma}$ has only one component directed along the vertical axis, $\boldsymbol{\gamma} = (0,0,\gamma)$:

$$\gamma = \frac{C_1(q)}{2} \left(\frac{\mathrm{Pm}}{1+\mathrm{Pm}} \right)^2 \mathrm{Re}^2 \, \alpha_* \, \mathrm{Sh}, \qquad (14)$$

$$\alpha_{12} = \alpha_{21} = \frac{C_1(q)}{10} \frac{(2\mathrm{Pm}+1)\,\mathrm{Pm}}{(1+\mathrm{Pm})^2} \mathrm{Re}^2 \, \alpha_* \, \mathrm{Sh}, \qquad (15)$$

where Sh $= \tau_{\rm f} S$ is the shear parameter. As follows from Eqs. (14) and (15), $\gamma \propto \mathrm{Pm}^2$ and $\alpha_{12} \propto \mathrm{Pm}$ for Pm $\ll 1$, while for Pm $\gg 1$ the effective pumping velocity γ and α_{12} are independent of Pm. For all values of the magnetic Prandtl numbers, γ and α_{12} are positive. This asymptotic behavior which is valid for Re $\ll 1$ is in agreement with Figs. 1 and 2 (see Sec. III). Note that the diagonal components of the tensor α_{ij} in this case are

$$\alpha = -\frac{C_2(q)}{3} \left(\frac{\mathrm{Rm}}{1+\mathrm{Pm}} \right) \tau_{\rm f} \langle \boldsymbol{u} \cdot (\nabla \times \boldsymbol{u}) \rangle^{(0)}, \qquad (16)$$

$$
\begin{aligned}
C_2(q) &= \int_{k_{\rm f}}^{k_{\rm d}} E(k) \left(\frac{k}{k_{\rm f}} \right)^{-2} dk \\
&= \left(\frac{q-1}{q+1} \right) \left[\frac{1 - (k_{\rm f}/k_{\rm d})^{q+1}}{1 - (k_{\rm f}/k_{\rm d})^{q-1}} \right]. \qquad (17)
\end{aligned}
$$

B. Large magnetic and hydrodynamic Reynolds numbers

To determine the the effective pumping velocity and the tensor α_{ij} in homogeneous helical turbulence with mean velocity shear for large magnetic and hydrodynamic Reynolds numbers we use the procedure which is similar to that applied in [9] in earlier investigations of shear flow turbulence. Let
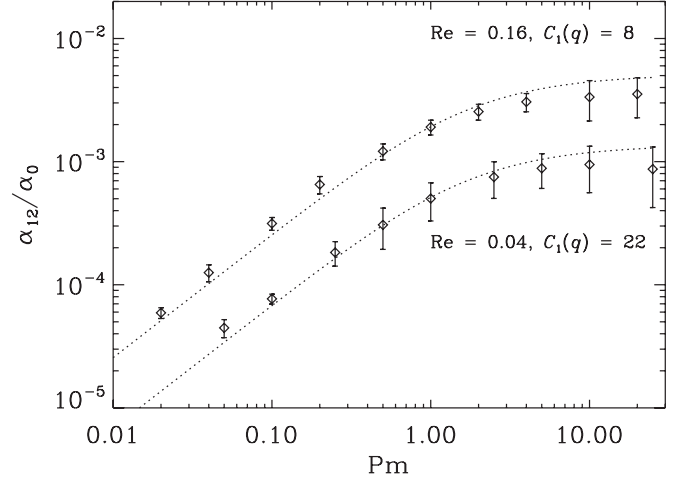

FIG. 2. Symmetric part of a_{ij}, $\alpha_{12} = \frac{1}{2}(a_{21} + a_{12})$ normalized by $\alpha_0 = \frac{1}{3} u_{\rm rms}$ as a function of Pm for the same runs as in Fig. 1. The dotted lines show the analytical result according to Eq. (15), with the values of $C_1(q)$ indicated in the legends.

us derive equations for the second moments. We apply the two-scale approach; e.g., we use large-scale $\boldsymbol{R} = (\boldsymbol{x} + \boldsymbol{y})/2$, $\boldsymbol{K} = \boldsymbol{k}_1 + \boldsymbol{k}_2$ and small-scale $\boldsymbol{r} = \boldsymbol{x} - \boldsymbol{y}$, $\boldsymbol{k} = (\boldsymbol{k}_1 - \boldsymbol{k}_2)/2$ variables (see, e.g., [28]). We derive equations for the following correlation functions:

$$f_{ij}(\boldsymbol{k}) = \hat{L}(u_i; u_j), \quad h_{ij}(\boldsymbol{k}) = \hat{L}(b_i; b_j),$$
$$g_{ij}(\boldsymbol{k}) = (4\pi\overline{\rho})^{-1} \hat{L}(b_i; u_j),$$

where

$$\hat{L}(a; c) = \int \langle a(\boldsymbol{k} + \boldsymbol{K}/2) c(-\boldsymbol{k} + \boldsymbol{K}/2) \rangle \, \exp(i\boldsymbol{K}\cdot\boldsymbol{R}) \, d\boldsymbol{K},$$

and $\langle ... \rangle$ denotes averaging over ensemble of turbulent velocity field. The equations for these correlation functions are given by (see [9])

$$\frac{\partial f_{ij}(\boldsymbol{k})}{\partial t} = i(\boldsymbol{k}\cdot\overline{\boldsymbol{B}})\Phi_{ij} + I_{ij}^f + I_{ijmn}^S(\overline{U}) f_{mn} + F_{ij} + \hat{\mathcal{N}} f_{ij},$$

$$\frac{\partial h_{ij}(\boldsymbol{k})}{\partial t} = -i(\boldsymbol{k}\cdot\overline{\boldsymbol{B}})\Phi_{ij} + I_{ij}^h + E_{ijmn}^S(\overline{U}) h_{mn} + \hat{\mathcal{N}} h_{ij},$$

$$
\begin{aligned}
\frac{\partial g_{ij}(\boldsymbol{k})}{\partial t} &= i(\boldsymbol{k}\cdot\overline{\boldsymbol{B}})\big[f_{ij}(\boldsymbol{k}) - h_{ij}(\boldsymbol{k}) - h_{ij}^{(H)} \big] + I_{ij}^g \\
&\quad + J_{ijmn}^S(\overline{U}) g_{mn} + \hat{\mathcal{N}} g_{ij}, \qquad (18)
\end{aligned}
$$

where hereafter we omit the arguments t and $\boldsymbol{R}$ in the correlation functions and neglect small terms $\sim O(\nabla^2)$. Here F_{ij} is related to the forcing term and $\nabla = \partial/\partial\boldsymbol{R}$. In Eqs. (18), $\Phi_{ij}(\boldsymbol{k}) = (4\pi\overline{\rho})^{-1} [g_{ij}(\boldsymbol{k}) - g_{ji}(-\boldsymbol{k})]$, and $\hat{\mathcal{N}} f_{ij}$, $\hat{\mathcal{N}} h_{ij}$, $\hat{\mathcal{N}} g_{ij}$ are the third-order moments appearing due to the nonlinear terms which include also molecular dissipation terms. The tensors $I_{ijmn}^S(\overline{U})$, $E_{ijmn}^S(\overline{U})$, and $J_{ijmn}^S(\overline{U})$ are given by

$$
\begin{aligned}
I_{ijmn}^S(\overline{U}) = \bigg(&2k_{iq}\delta_{mp}\delta_{jn} + 2k_{jq}\delta_{im}\delta_{pn} - \delta_{im}\delta_{jq}\delta_{pn} \\
&- \delta_{iq}\delta_{jn}\delta_{pm} + \delta_{im}\delta_{jn}k_q \frac{\partial}{\partial k_p} \bigg) \nabla_p \overline{U}_q,
\end{aligned}
$$

$$E_{ijmn}^{S}(\overline{U}) = \left(\delta_{im}\delta_{jq}\delta_{pn} + \delta_{jm}\delta_{iq}\delta_{pn}\right.$$
$$\left. + \delta_{im}\delta_{jn}k_q\frac{\partial}{\partial k_p}\right)\nabla_p\overline{U}_q,$$

$$J_{ijmn}^{S}(\overline{U}) = \left(2k_{jq}\delta_{im}\delta_{pn} - \delta_{im}\delta_{pn}\delta_{jq} + \delta_{jn}\delta_{pm}\delta_{iq}\right.$$
$$\left. + \delta_{im}\delta_{jn}k_q\frac{\partial}{\partial k_p}\right)\nabla_p\overline{U}_q,$$

where $k_{ij} = k_i k_j/k^2$. The source terms I_{ij}^{f}, I_{ij}^{h}, and I_{ij}^{g} which contain the large-scale spatial derivatives of the magnetic field $\overline{B}$ are given in [9]. Next, in Eqs. (18) we split the tensor for magnetic fluctuations into nonhelical, h_{ij}, and helical, $h_{ij}^{(H)}$, parts. The helical part of the tensor of magnetic fluctuations $h_{ij}^{(H)}$ depends on the magnetic helicity and it follows from magnetic helicity conservation arguments (see, e.g., [29–32] and [7] for a review).

The second-moment equations include the first-order spatial differential operators $\hat{\mathcal{N}}$ applied to the third-order moments $M^{(\mathrm{III})}$. A problem arises as to how to close the system, i.e., how to express the set of the third-order terms $\hat{\mathcal{N}}M^{(\mathrm{III})}$ through the lower moments $M^{(\mathrm{II})}$ (see, e.g., [33–35]). We use the spectral τ-closure approximation which postulates that the deviations of the third-moment terms, $\hat{\mathcal{N}}M^{(\mathrm{III})}(\boldsymbol{k})$, from the contributions to these terms due to the background turbulence, $\hat{\mathcal{N}}M^{(\mathrm{III},0)}(\boldsymbol{k})$, are expressed through the similar deviations of the second moments, $M^{(\mathrm{II})}(\boldsymbol{k}) - M^{(\mathrm{II},0)}(\boldsymbol{k})$:

$$\hat{\mathcal{N}}M^{(\mathrm{III})}(\boldsymbol{k}) - \hat{\mathcal{N}}M^{(\mathrm{III},0)}(\boldsymbol{k})$$
$$= -\frac{1}{\tau_r(k)}[M^{(\mathrm{II})}(\boldsymbol{k}) - M^{(\mathrm{II},0)}(\boldsymbol{k})] \qquad (19)$$

(see, e.g., [33,36,37]), where $\tau_r(k)$ is the scale-dependent relaxation time, which can be identified with the correlation time τ_{f} of the turbulent velocity field for large hydrodynamic and magnetic Reynolds numbers. The quantities with the superscript (0) correspond to the background shear-free turbulence with a zero mean magnetic field. We apply the spectral τ approximation only for the nonhelical part h_{ij} of the tensor of magnetic fluctuations. Note that a justification of the τ approximation for different situations has been performed in a number of numerical simulations and analytical studies (see, e.g., [7,38–45]).

We take into account that the characteristic time of variation of the magnetic field $\overline{B}$ is substantially longer than the correlation time τ_{f}. This allows us to obtain a stationary solution for Eqs. (18) for the second-order moments, $M^{(\mathrm{II})}(\boldsymbol{k})$, which are the sums of contributions caused by shear-free and sheared turbulence. The contributions to the mean electromotive force caused by a shear-free turbulence and sheared nonhelical turbulence are given in [9]. In particular, the contributions to the electromotive force caused by the sheared turbulence read $\mathcal{E}_m^{(S)} = \varepsilon_{mji}\int g_{ij}^{(S)}(\boldsymbol{k})\,d\boldsymbol{k}$, where the corresponding contributions to the cross-helicity tensor $g_{ij}^{(S)}$ in the kinematic approximation are given by

$$g_{ij}^{(S)}(\boldsymbol{k}) = i\,\tau_r(k)\left[J_{ijmn}^{S}\,\tau_r(k)\,(\boldsymbol{k}\cdot\overline{\boldsymbol{B}}) + \tau_r(k)\,(\boldsymbol{k}\cdot\overline{\boldsymbol{B}})\,I_{ijmn}^{S}\right]f_{mn}^{(0)},$$
$$(20)$$

and we use the following model for the background shear-free helical turbulence (with $\overline{B} = 0$):

$$f_{ij}^{(0)} = \langle u_i(\boldsymbol{k})\,u_j(-\boldsymbol{k},)\rangle^{(0)} = \left[\left(\delta_{ij} - \frac{k_i k_j}{k^2}\right)\langle\boldsymbol{u}^2\rangle^{(0)}\right.$$
$$\left. - \frac{i}{k^2}\,\varepsilon_{ijl}\,k_l\,\langle\boldsymbol{u}\cdot(\nabla\times\boldsymbol{u})\rangle^{(0)}\right]\frac{E(k)}{8\pi\,k^2}, \qquad (21)$$

where the energy spectrum is $E(k) = (q-1)\,(k/k_{\mathrm{f}})^{-q}$; $k_{\mathrm{f}} = 1/\ell_{\mathrm{f}}$ and the length ℓ_{f} is the maximum scale of turbulent motions. The turbulent correlation time is $\tau_r(k) = 2\,\tau_{\mathrm{f}}\,(k/k_{\mathrm{f}})^{1-q}$. Therefore, for large magnetic and hydrodynamic Reynolds number the effective pumping velocity $\boldsymbol{\gamma}$ and the off-diagonal components of the tensor α_{ij} caused by sheared helical turbulence are given by

$$\boldsymbol{\gamma} = \tfrac{2}{3}\,\tau_{\mathrm{f}}\,\alpha_*\,\overline{\boldsymbol{W}}, \qquad (22)$$
$$\alpha_{ij} = -\tfrac{4}{5}(5 - 2q)\,\tau_{\mathrm{f}}\,\alpha_*\,(\partial\overline{U})_{ij}. \qquad (23)$$

Since the mean symmetric tensor $(\partial\overline{U})_{ij}$ has only two nonzero components, $(\partial\overline{U})_{12} = (\partial\overline{U})_{21} = S/2$, the tensor α_{ij} has only two nonzero off-diagonal components, $\alpha_{12} = \alpha_{21}$. In particular,

$$\gamma = \tfrac{2}{3}\,\alpha_*\,\mathrm{Sh}, \qquad (24)$$
$$\alpha_{12} = \alpha_{21} = -\tfrac{2}{5}(5 - 2q)\,\alpha_*\,\mathrm{Sh} = -\tfrac{2}{3}\,\alpha_*\,\mathrm{Sh}, \qquad (25)$$

where we have used the Kolmogorov kinetic energy spectrum exponent $q = 5/3$ in Eq. (25). The diagonal components of the tensor α_{ij} in this case are $\alpha = \alpha_*$ (see, e.g., [1,3]). These results for large magnetic and hydrodynamic Reynolds number are in qualitative agreement with DNS performed in [25].

C. Large magnetic Reynolds numbers and small hydrodynamic Reynolds numbers

To develop a mean-field theory for large magnetic Reynolds numbers and small hydrodynamic Reynolds numbers we use stochastic calculus for a random velocity field. To derive an equation for the mean magnetic field we use an exact solution of the induction equation for the total field $\boldsymbol{B}$ (which is the sum of the mean $\overline{\boldsymbol{B}}$ and fluctuating $\boldsymbol{b}$ parts) with an initial condition $\boldsymbol{B}(t = t_0, \boldsymbol{x}) = \boldsymbol{B}(t_0, \boldsymbol{x})$ in the form of a functional integral:

$$B_i(t,\boldsymbol{x}) = \langle G_{ij}(t,t_0,\boldsymbol{\xi})\,\exp(\hat{\boldsymbol{\xi}}\cdot\nabla)B_j(t_0,\boldsymbol{x})\rangle_{\boldsymbol{w}} \qquad (26)$$

(see, e.g., [46,47]), where the operator $\exp(\hat{\boldsymbol{\xi}}\cdot\nabla)$ is determined by

$$\exp(\hat{\boldsymbol{\xi}}\cdot\nabla) = \sum_{k=0}^{\infty}\frac{1}{k!}\,(\hat{\boldsymbol{\xi}}\cdot\nabla)^k; \qquad (27)$$

$\hat{\boldsymbol{\xi}} = \boldsymbol{\xi} - \boldsymbol{x}$ (see Appendix B). The Wiener trajectory $\boldsymbol{\xi}(t,t_0,\boldsymbol{x})$ is determined by

$$\boldsymbol{\xi}(t,t_0,\boldsymbol{x}) = \boldsymbol{x} - \int_0^{t-t_0}\boldsymbol{v}(t_\sigma,\boldsymbol{\xi})\,d\sigma + (2\eta)^{1/2}\boldsymbol{w}(t - t_0), \qquad (28)$$

where $t_\sigma = t - \sigma$, and the velocity field $\boldsymbol{v}$ is the sum of the mean shear velocity $\overline{U}$ and fluctuating $\boldsymbol{u}$ parts. We consider large magnetic Reynolds number, but take into account small yet finite magnetic diffusion η. The magnetic diffusion can be described by a random Wiener process $\boldsymbol{w}(t)$

that is defined by the following properties: $\langle w_i(t) \rangle_w = 0$ and $\langle w_i(t+\tau) w_j(t) \rangle_w = \tau \delta_{ij}$, where $\langle \cdot \rangle_w$ denotes the averaging over the statistics of the Wiener random process. The function $G_{ij}(t,s,\boldsymbol{\xi})$ is determined by equation

$$\frac{dG_{ij}(t,s,\boldsymbol{\xi})}{ds} = N_{ik} G_{kj}(t,s,\boldsymbol{\xi}), \tag{29}$$

with the initial condition $G_{ij}(t=s) = \delta_{ij}$ and $N_{ij} = \nabla_j v_i$. The form of the exact solution (26) allows us to separate the averaging over random Brownian motion of particles [i.e., the averaging over a random Wiener process $\boldsymbol{w}(t)$] and a random velocity $\boldsymbol{u}$.

We consider a random flow with a small yet finite Strouhal number (that is the ratio the correlation time of a random fluid flow to the turnover time $\ell_f / u_{\rm rms}$). A random velocity field with a small Strouhal number can be modeled by a random velocity field with a constant renewal time τ. Assume that in the intervals $\ldots(-\tau,0);(0,\tau);(\tau,2\tau);\ldots$ the velocity fields are statistically independent and have the same statistics. This implies that the velocity field looses memory at the prescribed instants $t = m\tau$, where $m = 0, \pm 1, \pm 2, \ldots$. This velocity field cannot be considered as a stationary velocity field for small times $\sim \tau$; however, it behaves like a stationary field for $t \gg \tau$. Averaging Eq. (26) over the random velocity field we arrive at the equation for the mean magnetic field, $\overline{\boldsymbol{B}}$:

$$\frac{\partial \overline{B}_i}{\partial t} = [\nabla \times (\overline{\boldsymbol{U}} \times \overline{\boldsymbol{B}})]_i + A_{ijm} \nabla_m \overline{B}_j + D_{ijmn} \nabla_m \nabla_n \overline{B}_j \tag{30}$$

(see Appendix B), where

$$A_{ijm} = \frac{1}{\tau} \langle \langle \hat{\xi}_m \, G_{ij} \rangle \rangle_w, \tag{31}$$

$$D_{ijmn} = \frac{1}{2\tau} \langle \langle \hat{\xi}_m \hat{\xi}_n \, G_{ij} \rangle \rangle_w; \tag{32}$$

the angular brackets $\langle \cdot \rangle$ denote an ensemble average over the random velocity field. Therefore, the mean magnetic field is determined by double averaging over two independent random processes, i.e., by the ensemble average over the random velocity field and by the average over Wiener random process $\boldsymbol{w}(t)$.

We are interested in the lowest order contributions to the mean electromotive force which are proportional to the mean magnetic field, $\mathcal{E}_i^{(a)} = a_{ij} \overline{B}_j$, where $a_{ij} = (1/2)\varepsilon_{inm} A_{njm}$ and the tensor A_{ijm} reads

$$A_{ijm} = -\frac{1}{\tau} \int_0^\tau dt \int_0^\tau dt' \langle [v_m(t,\boldsymbol{\xi})]_{\bf x} [\nabla_j v_i(t',\boldsymbol{\xi})]_{\bf y} \rangle, \tag{33}$$

where ${\bf x} \to {\bf y}$ and $[v_m(t,\boldsymbol{\xi})]_{\bf x}$ denotes the Eulerian velocity determined at the Wiener trajectory $\boldsymbol{\xi}$ that passes through the point ${\bf x}$ at instant t. Hereafter the angular brackets denote double averaging over a random velocity field and over the statistics of the Wiener process.

For small hydrodynamic Reynolds numbers we seek the solutions of the linearized Navier-Stokes equation (2) for incompressible velocity field $\boldsymbol{u}$ as superpositions of the Orr-Kelvin random shearing waves $\boldsymbol{u}(t,\boldsymbol{r}) = \int \boldsymbol{u}(t,\boldsymbol{k}_0) \exp[i\,\boldsymbol{k}(t)\cdot\boldsymbol{r}] \, d\boldsymbol{k}_0$,

where $\boldsymbol{k}_0 = (k_{x0},k_y,k_z)$, $\boldsymbol{k}(t) = (k_{x0} - Sk_y t, k_y, k_z)$ (see, e.g., [23,48–50]). Therefore, the effective pumping velocity $\boldsymbol{\gamma}$ and the off-diagonal components of the tensor α_{ij} are given by

$$\gamma_n = \frac{1}{2} \varepsilon_{nji} a_{ij} = \frac{1}{4} A_{kmm} = -\frac{i}{4\tau} \int_0^\tau dt \int_0^\tau dt'$$
$$\times k_m(t') \langle v_m(t,\boldsymbol{k}_0) \, v_n^*(t',\boldsymbol{k}_0) \rangle, \tag{34}$$

$$\alpha_{ij} = \frac{1}{2}(a_{ij} + a_{ji}) = \frac{1}{4}(\varepsilon_{inm} A_{njm} + \varepsilon_{jnm} A_{nim})$$
$$= -\frac{i}{4\tau} \int_0^\tau dt \int_0^\tau dt' \, [\varepsilon_{inm} k_j(t') + \varepsilon_{jnm} k_i(t')]$$
$$\times \langle v_m(t,\boldsymbol{k}_0) \, v_n^*(t',\boldsymbol{k}_0) \rangle. \tag{35}$$

Using these equations and Eqs. (C13)–(C10) in Appendix C we obtain the effective pumping velocity $\boldsymbol{\gamma} = (0,0,\gamma)$ and the off-diagonal components $\alpha_{12} = \alpha_{21}$ of the tensor α_{ij} for large magnetic Reynolds numbers and small hydrodynamic Reynolds numbers:

$$\gamma = \frac{C_1(q)}{3} \alpha_* \, {\rm Sh} \, {\rm Re}^2, \tag{36}$$

$$\alpha_{12} = \alpha_{21} = \left(C_2(q) \, {\rm Re} \, \frac{\tau}{\tau_{\rm f}} - \frac{3 \, C_1(q)}{2} \, {\rm Re}^2 \right) \alpha_* \, {\rm Sh}, \tag{37}$$

where ${\rm Re} \ll \tau/\tau_{\rm f} < 1$. The diagonal components of the tensor α_{ij} in this case obtained using the path-integral approach are $\alpha = -(1/3) \langle \tau \boldsymbol{u} \cdot (\nabla \times \boldsymbol{u}) \rangle^{(0)}$ (see, e.g., [46,51]). In the next section we discuss comparison with new systematic DNS designed for comparison with our theoretical predictions.

III. COMPARISON WITH DNS

A. Numerical model

Our DNS model is identical to that used in [25]. We begin by testing the analytical results numerically using three-dimensional simulations of isotropically forced turbulence in a fully periodic cube of size $(2\pi)^3$. The uniform shear $\overline{\boldsymbol{U}} = (0,Sx,0)$ is imposed using the shearing box method and the gas obeys an isothermal equation of state characterized by the constant speed of sound $c_{\rm s}$. We solve the continuity and Navier-Stokes equations in the form

$$\frac{\mathcal{D}\ln\rho}{\mathcal{D}t} = -\boldsymbol{U} \cdot \nabla \ln\rho - \nabla \cdot \boldsymbol{U}, \tag{38}$$

$$\frac{\mathcal{D}\boldsymbol{U}}{\mathcal{D}t} = -\boldsymbol{U} \cdot \nabla \boldsymbol{U} - SU_x \hat{\boldsymbol{y}} - c_{\rm s}^2 \nabla \ln\rho + \boldsymbol{f} + \boldsymbol{F}_{\rm visc}, \tag{39}$$

where the imposed shear is subsumed in the advective derivative

$$\frac{\mathcal{D}}{\mathcal{D}t} \equiv \frac{\partial}{\partial t} + Sx \frac{\partial}{\partial y}. \tag{40}$$

Here ρ is the density, $\boldsymbol{U}$ is the velocity, $\boldsymbol{f}$ describes the forcing, and $\boldsymbol{F}_{\rm visc} = \rho^{-1} \nabla \cdot (2\rho\nu{\sf S})$ is the viscous force, where ν is the kinematic viscosity, and

$${\sf S}_{ij} = \tfrac{1}{2}(U_{i,j} + U_{j,i}) - \tfrac{1}{3}\nabla \cdot \boldsymbol{U}\delta_{ij} \tag{41}$$

is the traceless rate of strain tensor. The forcing function $\boldsymbol{f}$ is given in [52]:

$$\boldsymbol{f}(\boldsymbol{x},t) = \mathrm{Re}\{N \boldsymbol{f}_{\boldsymbol{k}(t)} \exp[i\boldsymbol{k}(t) \cdot \boldsymbol{x} + i\phi(t)]\}, \quad (42)$$

where $\boldsymbol{x}$ is the position vector. The wave vector $\boldsymbol{k}(t)$ and the random phase $-\pi < \phi(t) \leqslant \pi$ change at every time step, so $\boldsymbol{f}(\boldsymbol{x},t)$ is δ-correlated in time. The normalization factor N is chosen on dimensional grounds to be $N = f_0 c_s(|\boldsymbol{k}|c_s/\delta t)^{1/2}$, where f_0 is a nondimensional forcing amplitude. At each time step we select randomly one of many possible wave vectors in a certain range around a given forcing wave number. The average wave number is referred to as k_f. In the present study we always use $k_f/k_1 = 5$. We force the system with transverse helical waves [53],

$$\boldsymbol{f}_{\boldsymbol{k}} = \mathsf{R} \cdot \boldsymbol{f}_{\boldsymbol{k}}^{(\mathrm{nohel})} \quad \text{with} \quad \mathsf{R}_{ij} = \frac{\delta_{ij} - i\sigma\epsilon_{ijk}\hat{k}_k}{\sqrt{1+\sigma^2}}, \quad (43)$$

where $\sigma = 1$ for the fully helical case with positive helicity of the forcing function,

$$\boldsymbol{f}_{\boldsymbol{k}}^{(\mathrm{nohel})} = (\boldsymbol{k} \times \hat{\boldsymbol{e}})/\sqrt{\boldsymbol{k}^2 - (\boldsymbol{k} \cdot \hat{\boldsymbol{e}})^2} \quad (44)$$

is a nonhelical forcing function, and $\hat{\boldsymbol{e}}$ is an arbitrary unit vector not aligned with $\boldsymbol{k}$; note that $|\boldsymbol{f}_{\boldsymbol{k}}|^2 = 1$. We use fully helical forcing, i.e., $\sigma = 1$, in all of our runs.

The boundary conditions in the y and z directions are periodic, whereas shearing-periodic conditions are used in the x direction. The simulations are governed by the fluid and magnetic Reynolds numbers, the magnetic Prandtl number, and the shear and Mach numbers:

$$\mathrm{Re} = \frac{u_{\mathrm{rms}}}{\nu k_f}, \quad \mathrm{Rm} = \frac{u_{\mathrm{rms}}}{\eta k_f}, \quad \mathrm{Pm} = \frac{\nu}{\eta},$$

$$\mathrm{Sh} = \frac{S}{u_{\mathrm{rms}}k_f}, \quad \mathrm{Ma} = \frac{u_{\mathrm{rms}}}{c_s}. \quad (45)$$

Here u_{rms} is the root-mean-square velocity of turbulent motions and η is the magnetic diffusivity. We use the PENCIL CODE[1] to perform the simulations.

B. Test-field method

We apply the kinematic test-field method (see, e.g., [15,54,55]) to compute the effective pumping velocity $\boldsymbol{\gamma}$ and all components of the tensor α_{ij}. The essence of this method is that a set of prescribed test fields $\overline{\boldsymbol{B}}^{(p,q)}$ and the flow from the DNS are used to evolve separate realizations of small-scale fields $\boldsymbol{b}^{(p,q)}$. Neither the test fields $\overline{\boldsymbol{B}}^{(p,q)}$ nor the small-scale fields $\boldsymbol{b}^{(p,q)}$ act back on the flow. These small-scale fields are then used to compute the electromotive force $\overline{\boldsymbol{\mathcal{E}}}^{(p,q)}$ corresponding to the test field $\overline{\boldsymbol{B}}^{(p,q)}$. The number and form of the test fields used depends on the problem at hand. For the purposes of the present study we use uniform horizontal test fields $\overline{\boldsymbol{B}}^{(1)} = (B_0,0,0)$ and $\overline{\boldsymbol{B}}^{(2)} = (0,B_0,0)$, in which case the series expansion of the electromotive force contains only a single term

$$\mathcal{E}_i^{(a)} = a_{ij}\overline{B}_j. \quad (46)$$

_____

[1]See http://pencil-code.googlecode.com.

TABLE I. Summary of the runs.

Set	Re	Pm	Sh	Ma	Grid
A1	0.04	0.05...25	-0.20	0.010	$32^3 \ldots 64^3$
A2	0.16	0.02...20	-0.13	0.016	$32^3 \ldots 64^3$
B1	0.08...81	1	-0.025	0.080	$32^3 \ldots 256^3$
B2	0.08...83	1	-0.075	0.080	$32^3 \ldots 256^3$
B3	0.08...3.5	1	-0.25	0.080	32^3
B4	0.08...0.4	1	-2.5	0.080	32^3
C1	0.04	1	$-0.020\ldots-0.19$	0.010	32^3
C2	0.16	1	$-0.012\ldots-0.12$	0.016	32^3
C3	0.45	1	$-0.009\ldots-0.09$	0.023	32^3
C4	1.3	1	$-0.006\ldots-0.07$	0.032	32^3
D1	0.08	1	-0.010	0.002...0.41	32^3

We present the results using the quantities

$$\alpha = \tfrac{1}{2}(a_{11} + a_{22}), \quad (47)$$

$$\alpha_{12} = \alpha_{21} = \tfrac{1}{2}(a_{21} + a_{12}), \quad (48)$$

$$\gamma = \tfrac{1}{2}(a_{21} - a_{12}). \quad (49)$$

We use $\alpha_0 = \tfrac{1}{3}u_{\mathrm{rms}}$ as a normalization factor when presenting numerical results. Errors are estimated by dividing the time series into three equally long parts and computing time averages for each of them. The largest departure from the time average computed over the entire time series represents the error. This definition of the error bar gives an indication about the mean value that one would obtain for shorter parts of the time series. With this definition, the error bars do normally become shorter for longer runs, provided the time series is stationary. This would not be the case for the rms value of the deviations, which might sometimes also be of interest.

C. Results

We perform several sets of simulations where we vary the parameters Pm, Rm, Sh, and Ma individually to study the analytical results derived in Sec. II; see Table I. The setup used here is prone to exhibit the so-called vorticity dynamo [10,24], due to which large-scale vorticity is generated, and complications can arise in the interpretation of the simulation data. Here we restrict the studied parameter range so that the values of Re and Sh are subcritical for the vorticity dynamo. In our runs where the Reynolds numbers are of the order of unity or less, a low grid resolution of 32^3 is often sufficient. Indeed, in Table II we show the results obtained for different resolutions ranging from 16^3 to 128^3 for Rm around 1, which demonstrates good convergence of the results within error bars.

TABLE II. Convergence study of γ and α_{21} for Rm = 1.3 and Sh = -0.06 from simulations with different grid sizes.

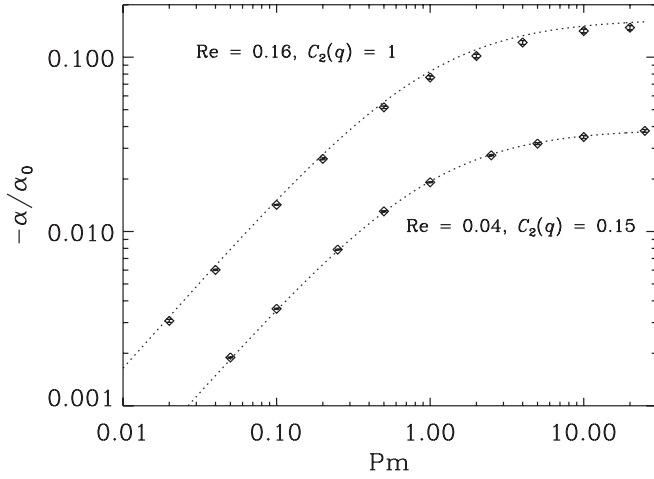| Run	γ/α_0 (10^{-2})	α_{21}/α_0 (10^{-2})	Grid
E1	1.02 ± 0.12	0.94 ± 0.25	16^3
E2	1.05 ± 0.07	0.89 ± 0.20	32^3
E3	0.99 ± 0.06	0.83 ± 0.55	64^3
E4	0.94 ± 0.18	0.88 ± 0.23	128^3

FIG. 3. α effect as a function of Pm normalized by $\alpha_0 = \frac{1}{3}u_{rms}$ for the same runs as in Fig. 1. Analytical results according to Eq. (16) are overplotted with dotted lines. The values of $C_2(q)$ are used as fit parameters and indicated in the legends.

1. Dependence on **Pm**

Figure 1 shows our results for γ as a function of magnetic Prandtl number Pm. We find that the numerical results coincide with the analytical formula, Eq. (14). Values of the order of $C_1(q) \approx 1$ fit the DNS results within the error estimates.

Figure 2 shows the results for α_{12} as a function of Pm for two values of Re. The data for α_{12} shows significantly larger fluctuations than the corresponding results for γ. However, the DNS results seem to fall in line with the analytical expression, Eq. (15), although the value of $C_1(q)$ needed to fit the data is an order of magnitude larger than in the case of γ. This can be explained by comparing Eqs. (36) and (37), which show that $\gamma \propto \mathrm{Re}^2$, while $\alpha_{12} \propto \mathrm{Re}\,(\tau/\tau_f)$, where τ is the flow renovating time, and $\tau_f = \ell_f/u_{rms}$ is the turnover time of turbulent eddies. Note that Eqs. (36) and (37) are obtained for large magnetic Reynolds numbers, while $\mathrm{Re} \ll \tau/\tau_f < 1$.
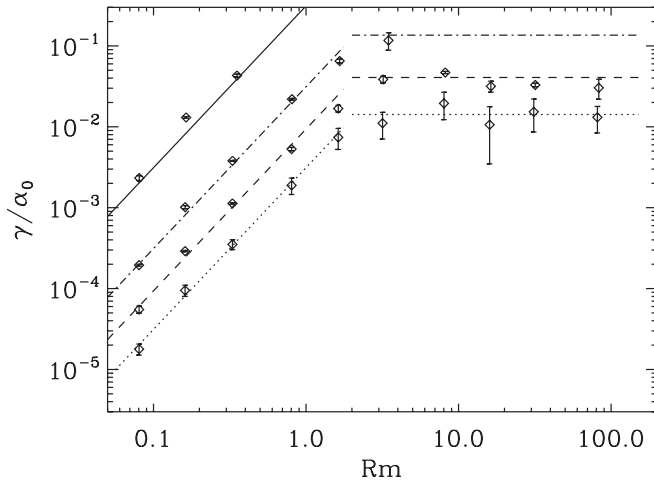

FIG. 4. γ as a function of Rm for Pm = 1 and for four values of Sh (-0.025, -0.075, -0.25, and -2.5; see Sets B1 to B4). The lines show the analytical results according to Eqs. (14) and (24) with $C_1(q) = 1$, for Sets B1 (dotted lines), B2 (dashed), B3 (dot-dashed), and B4 (triple-dot dashed), respectively.
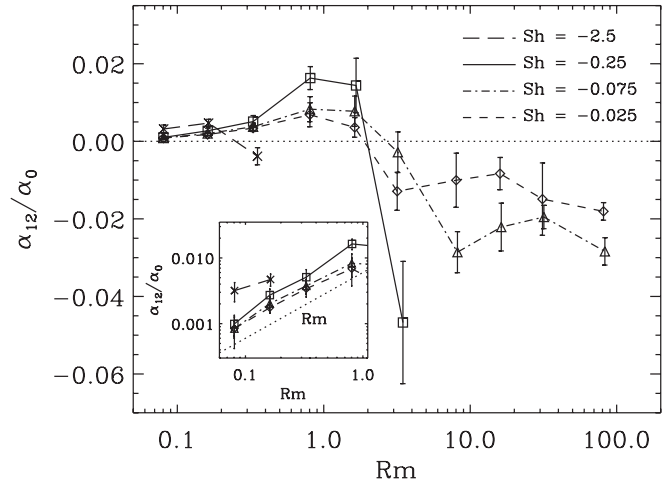

FIG. 5. Symmetric contribution α_{12} as a function of Rm for Pm = 1 and four values of shear as indicated by the legend (Sets B1 to B4).

This implies that for these conditions $\alpha_{12} \gg \gamma$. The latter is in agreement with DNS results (see Figs. 1 and 2).

In Fig. 3 we show the α effect (the diagonal elements of the α_{ij} tensor) as a function of the magnetic Prandtl number Pm. These results are in a good agreement with the analytical results (16).

2. Dependence on **Rm**

Our results for γ as a function of Rm are shown in Fig. 4. We find that for Rm smaller than roughly two, γ is well described by the analytical result, Eq. (14), obtained for Rm $\ll$ 1 and Re $\ll$ 1. For greater Rm, γ is consistent with a constant value as a function of Rm and is in accordance with Eq. (24) derived for Rm $\gg$ 1 and Re $\gg$ 1. Note also that for the largest values of the shear parameter, Sh $= -2.5\,(-0.25)$, there is a vorticity dynamo for Rm > 1 (Rm > 3), so no points are plotted in those cases.

The off-diagonal component α_{12}, shown in Fig. 5, is proportional to Re for small Rm, while the analytical expression
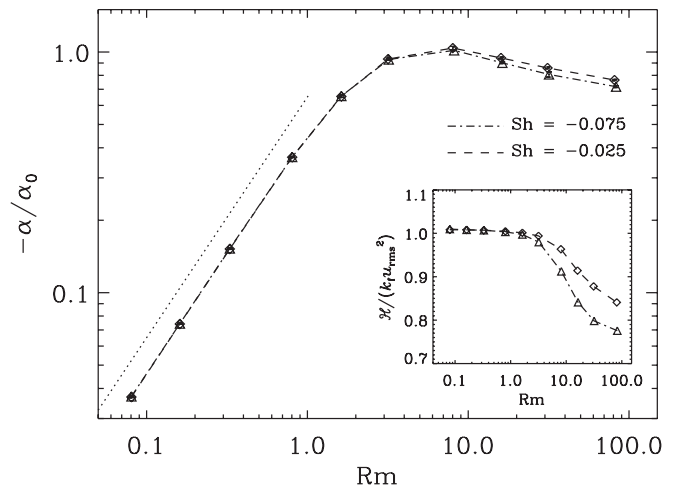

FIG. 6. α effect as a function of Rm normalized by $\alpha_0 = \frac{1}{3}u_{rms}$ for two values of Re (Sets B1 and B2). The dotted line is proportional to Rm. The inset shows the normalized kinetic helicity of the flow.
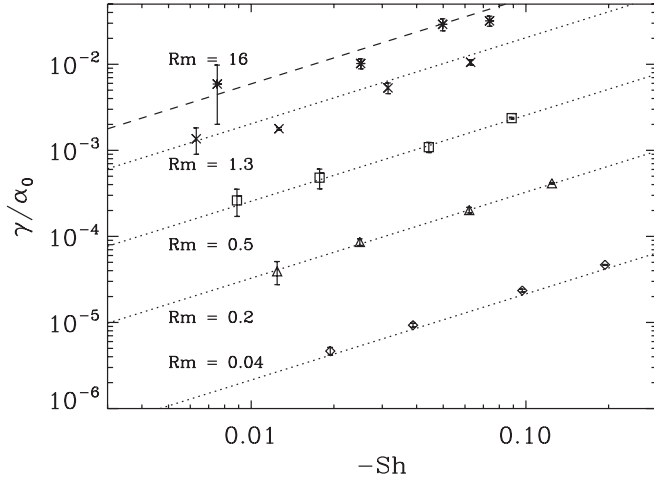
FIG. 7. Pumping velocity $\gamma = \frac{1}{2}(a_{21} - a_{12})$ normalized by α_0 as a function of Sh for Pm = 1 and different values of Rm as indicated in the legend (Sets C1–C4). Analytical results according to Eqs. (14) with $C_1(q) = 1$, and (24) are overplotted with dotted and dashed lines, respectively.

(15) yields $\alpha_{12} \propto \mathrm{Re}^2$. A sign change occurs for Rm ≈ 2, and the values of α_{12} are consistently negative in this regime in agreement with Eq. (25) derived for Rm $\gg 1$ and Re $\gg 1$. The data are noisy but suggest that α_{12} could be independent of Rm at high Rm in agreement with the analytical result (25). Furthermore, for small Rm the dependence on shear is weak, although a clearer dependence on shear is seen for Rm greater than around 10.

In Fig. 6 we show α as a function of Rm. We find that α is proportional to Rm for small magnetic Reynolds numbers in agreement with Eq. (16). For Rm greater than roughly five, α decreases slightly, while the theory suggests that α is independent of Rm for Rm $\gg 1$. This inconsistency can be understood in terms of the relative kinetic helicity $\mathcal{H}/(k_{\mathrm{f}} u_{\mathrm{rms}}^2)$, where $\mathcal{H} = \overline{\boldsymbol{\omega} \cdot \boldsymbol{u}}$, which decreases by about 20
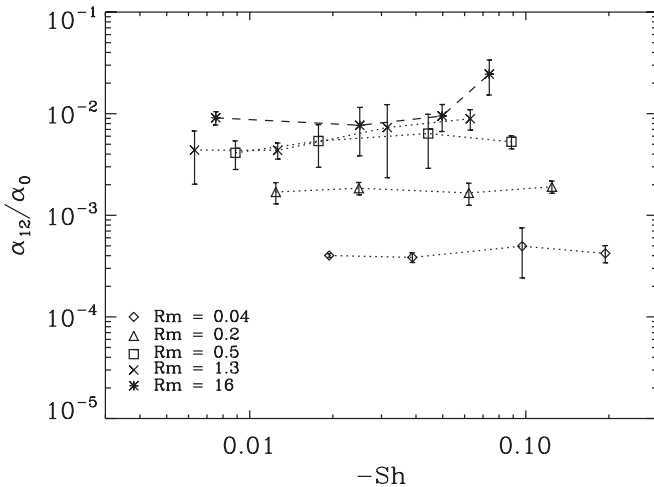

FIG. 8. Symmetric contribution α_{12} normalized by α_0 as a function of Sh for Pm = 1 and different values of Rm as indicated in the legend (Sets C1–C4). Runs with Rm = 16 are shown with asterisks and connected by a dashed line. For these runs $\alpha_{12} < 0$ so the plot shows $-\alpha_{12}$.
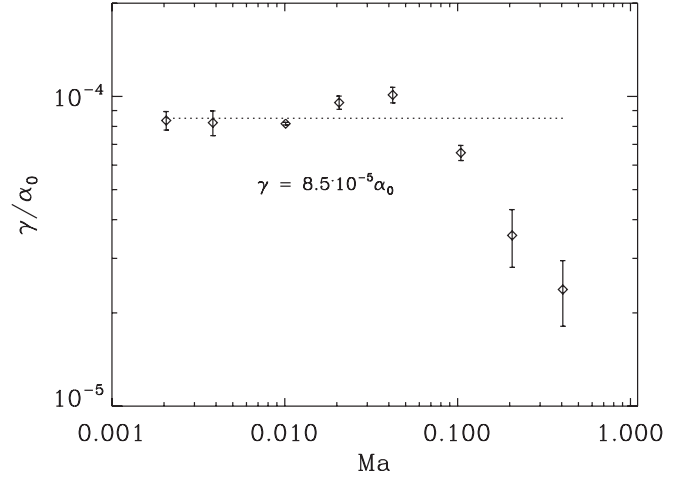

FIG. 9. Pumping coefficient $\gamma = \frac{1}{2}(a_{21} - a_{12})$ as a function of the Mach number for Pm = 1 (Set D1). The normalization factor is $\alpha_0 = \frac{1}{3} u_{\mathrm{rms}}$, and Sh = -0.10.

percent between Rm 8 and 83 (see the inset in Fig. 6). Since $\alpha \propto \mathcal{H}$, this explains the decrease of α with Rm for Rm $\gg 1$.

3. Dependence on shear

Figure 7 shows the pumping velocity γ normalized by α_0 as a function of the shear number, Sh, for Pm = 1 and different values of Rm. Linear dependence of γ on shear is clearly seen in Fig. 7. This is in agreement with the analytical result of Eq. (14). Rather surprisingly, the data for α_{12} suggest that there is no dependence on shear (Fig. 8), in contradiction with the analytical result of Eq. (15) that was derived for small shear, $S\tau_{\mathrm{f}} \ll 1$.

Note that our theory has been developed for incompressible flow since the DNS results are nearly independent of Mach number for Ma < 0.05. This is shown in Fig. 9, where we notice a sharp decline of γ for larger values of the Mach number. We are not aware of similar findings for mean-field transport coefficients as a function of Mach number.

IV. DISCUSSION AND CONCLUSIONS

To clarify the physical effect related to the pumping velocity $\boldsymbol{\gamma}$ and the off-diagonal components of the tensor α_{ij} we rewrite the contributions to the mean electromotive force which are proportional to the mean magnetic field in the following form:

$$\mathcal{E}_i^{(S)} = \alpha_{ij} \overline{B}_j + (\boldsymbol{\gamma} \times \overline{\boldsymbol{B}})_i$$
$$= [\boldsymbol{\gamma}^{(P)} \times \overline{\boldsymbol{B}}^{(P)} + \boldsymbol{\gamma}^{(T)} \times \overline{\boldsymbol{B}}^{(T)}]_i, \qquad (50)$$

where $\overline{\boldsymbol{B}}^{(T)}$ is the toroidal mean magnetic field directed along the mean shear velocity $\overline{U}$ (along the y axis), $\overline{\boldsymbol{B}}^{(P)}$ is the poloidal mean magnetic field directed perpendicular to both the mean shear velocity $\overline{U}$ and the mean vorticity (along the x axis), while the pumping velocities $\boldsymbol{\gamma}^{(T)}$ and $\boldsymbol{\gamma}^{(P)}$ of the toroidal and poloidal components of the mean magnetic field are given by

$$\boldsymbol{\gamma}^{(P)} = \hat{\boldsymbol{z}} (\alpha_{12} + \gamma), \qquad (51)$$
$$\boldsymbol{\gamma}^{(T)} = -\hat{\boldsymbol{z}} (\alpha_{12} - \gamma). \qquad (52)$$

Here we take into account the following identities for the off-diagonal components of the tensor $\alpha_{ij} = (\hat{x}_i \hat{y}_j + \hat{x}_j \hat{y}_i)\, \alpha_{12}$ and $\alpha_{ij} \overline{B}_j = \alpha_{12}\, \hat{z} \times (\overline{\boldsymbol{B}}^{(P)} - \overline{\boldsymbol{B}}^{(T)})$, where $\alpha_{12} = \alpha_{21}$ and $\hat{\boldsymbol{x}}$, $\hat{\boldsymbol{y}}$, $\hat{\boldsymbol{z}}$ are the unit vectors directed along the x, y, and z axes, respectively.

It follows from these equations that when $\alpha_{12} > \gamma > 0$, the effective pumping velocity of the poloidal mean magnetic field is directed upward (along the z axis), while the effective pumping velocity of the toroidal mean magnetic field is directed downward. When $\alpha_{12} < 0$, but $|\alpha_{12}| > \gamma$, the situation is the opposite, i.e., the effective pumping velocity of the toroidal mean magnetic field is directed upward, while the effective pumping velocity of the poloidal mean magnetic field is directed downward. Therefore, the effective pumping velocity γ and the off-diagonal components of the tensor α_{ij} result in a separation of toroidal and poloidal components of the mean magnetic field. This effect is very important for large-scale dynamo action in shear flow turbulence.

Another reason for the different pumping velocity of toroidal and poloidal components of the mean magnetic field is a combination of the effects of rotation and stratification on small-scale turbulence. The effect of the separation of toroidal and poloidal components of the mean magnetic field was early identified in analytic calculations of rotating stratified turbulence in [26,56], confirmed in DNS of rotating stratified convection [57,58], and included in numerical mean-field modeling of the solar dynamo in [59]. Note also that a nonlinear feedback of the mean magnetic field to turbulent fluid flow causes a different pumping velocity of toroidal and poloidal components of the mean magnetic field [9]. The latter effect was included in numerical mean-field modeling of the solar dynamo in [60].

In summary, we have developed a mean-field theory for a pumping effect of the mean magnetic field in homogeneous helical turbulence with imposed large-scale shear. In our analysis we use the quasilinear approach, the path-integral technique, and the tau-relaxation approximation, which allow us to determine all components of the α tensor in different ranges of hydrodynamic and magnetic Reynolds numbers. The pumping effect depends on the α effect and on shear. Using DNS and the kinematic test-field method we were able to determine all components of the α tensor from numerical simulations of sheared helical turbulence. The majority of the numerical results for the effective pumping velocity and the diagonal and off-diagonal components of the α tensor are in good agreement with the theoretical results. However, the numerical results for α_{12} suggest that there is no dependence of the off-diagonal component on shear in contradiction with the analytical result. In addition, according to the numerical results $\alpha_{12}(\mathrm{Re})$ is proportional to Re for small Rm, while the theory yields $\alpha_{12} \propto \mathrm{Re}^2$. On the other hand, the change of the sign of α_{12} from positive for small Rm to negative for large Rm observed in DNS is in agreement with the theoretical predictions.

APPENDIX A: THE INTEGRALS OF THE GREEN'S FUNCTIONS

For the integration in ω space in the case of small magnetic and hydrodynamic Reynolds numbers we used the following integrals in Eqs. (11) and (12):

$$I_0(k) = \int G_\eta \, G_\nu \, G_\nu^* \, d\omega = \frac{\pi}{\nu\,(\nu + \eta)\,k^4},$$

$$I_1(k) = \int G_\eta^2 \, G_\nu^2 \, G_\nu^* \, d\omega = \frac{\pi}{2\,\nu^2\,(\nu + \eta)^2\,k^8},$$

$$I_2(k) = \int G_\eta^2 \, G_\nu \, (G_\nu^*)^2 \, d\omega = \frac{\pi\,(5\nu + \eta)}{2\,\nu^2\,(\nu + \eta)^3\,k^8},$$

$$I_3(k) = \int G_\eta \, G_\nu \, (G_\nu^*)^3 \, d\omega = \frac{\pi}{4\,\nu^3\,(\nu + \eta)^3\,k^8}$$
$$\times [2\nu(\nu + \eta) + (\nu + \eta)^2 + 4\nu^2],$$

$$I_4(k) = \int G_\eta \, G_\nu \, (G_\nu^*)^2 \, d\omega = \frac{\pi\,(3\nu + \eta)}{2\,\nu^2\,(\nu + \eta)^2\,k^6},$$

$$I_5(k) = \int G_\eta \, G_\nu^2 \, G_\nu^* \, d\omega = \frac{\pi}{2\,\nu^2\,(\nu + \eta)\,k^6},$$

$$I_6(k) = \int G_\eta \, G_\nu^3 \, G_\nu^* \, d\omega = \frac{\pi}{4\,\nu^3\,(\nu + \eta)\,k^8},$$

$$I_7(k) = \int G_\eta^3 \, G_\nu \, G_\nu^* \, d\omega = \frac{\pi}{\nu\,(\nu + \eta)^3\,k^8},$$

$$I_8(k) = \int G_\eta^2 \, G_\nu \, G_\nu^* \, d\omega = \frac{\pi}{\nu\,(\nu + \eta)^2\,k^6}.$$

APPENDIX B: DERIVATION OF EQS. (26) AND (30) IN PATH-INTEGRAL APPROACH

To derive Eq. (26) we use an exact solution of the induction equation with an initial condition $\boldsymbol{B}(t = t_0, \boldsymbol{x}) = \boldsymbol{B}(t_0, \boldsymbol{x})$ in the form of the Feynman-Kac formula,

$$B_i(t, \boldsymbol{x}) = \langle G_{ij}(t, t_0, \boldsymbol{\xi})\, B_j(t_0, \boldsymbol{\xi}) \rangle_{\boldsymbol{w}}, \qquad \text{(B1)}$$

and assume that

$$B_j(t_0, \boldsymbol{\xi}) = \int \exp(i \boldsymbol{\xi} \cdot \boldsymbol{q}) B_j(t_0, \boldsymbol{q})\, d\boldsymbol{q}. \qquad \text{(B2)}$$

Substituting Eq. (B2) into Eq. (B1) we obtain

$$B_i(t, \boldsymbol{x}) = \int \langle G_{ij}(t, t_0, \boldsymbol{\xi})\, \exp[i \hat{\boldsymbol{\xi}} \cdot \boldsymbol{q}] \rangle_{\boldsymbol{w}}$$
$$\times B_j(t_0, \boldsymbol{q})\, \exp(i \boldsymbol{q} \cdot \boldsymbol{x})\, d\boldsymbol{q}, \qquad \text{(B3)}$$

where $\hat{\boldsymbol{\xi}} = \boldsymbol{\xi} - \boldsymbol{x}$. In Eq. (B3) we expand the function $\exp[i\hat{\boldsymbol{\xi}} \cdot \boldsymbol{q}]$ in Taylor series at $\boldsymbol{q} = 0$,

$$\exp(i\hat{\boldsymbol{\xi}} \cdot \boldsymbol{q}) = \sum_{k=0}^{\infty} \frac{1}{k!} (i\hat{\boldsymbol{\xi}} \cdot \boldsymbol{q})^k,$$

and use the identity

$$\nabla^k \exp(i\boldsymbol{x} \cdot \boldsymbol{q}) = (i\boldsymbol{q})^k \exp(i\boldsymbol{x} \cdot \boldsymbol{q}).$$

This allows us to rewrite Eq. (B3) as follows:

$$B_i(t,\boldsymbol{x}) = \left\langle G_{ij}(t,t_0,\boldsymbol{\xi}) \left[\sum_{k=0}^{\infty} \frac{1}{k!} (\hat{\boldsymbol{\xi}} \cdot \nabla)^k \right] \right\rangle_{\boldsymbol{w}}$$
$$\times \int B_j(t_0,\boldsymbol{q}) \exp(i\boldsymbol{q} \cdot \boldsymbol{x}) \, d\boldsymbol{q}. \quad (B4)$$

After the inverse Fourier transformation, $B_j(t_0,\boldsymbol{x}) = \int B_j(t_0,\boldsymbol{q}) \exp(i\boldsymbol{q} \cdot \boldsymbol{x}) \, d\boldsymbol{q}$, in Eq. (B4) we obtain Eq. (26). Equation (B2) can be formally considered as an inverse Fourier transformation of the function $B_j(t_0,\boldsymbol{\xi})$. Equation (26) has been also derived by a rigorous method, using the Feynman-Kac formula and Cameron-Martin-Girsanov theorem (see [47]).

Averaging Eq. (26) over the random velocity field yields the equation for the mean magnetic field

$$\overline{B}_i((m+1)\tau,\boldsymbol{x}) = \langle\langle G_{ij}(t,s,\boldsymbol{\xi}) \exp(\hat{\boldsymbol{\xi}} \cdot \nabla)\rangle\rangle_{\boldsymbol{w}} \overline{B}_j(m\tau,\boldsymbol{x}),$$
$$(B5)$$

where the angular brackets $\langle \cdot \rangle$ denote the ensemble average over the random velocity field. Now we use the identity

$$\overline{B}_i(t+\tau,\boldsymbol{x}) = \exp\left(\tau \frac{\partial}{\partial t}\right) \overline{B}_i(t,\boldsymbol{x}), \quad (B6)$$

which follows from the Taylor expansion

$$f(t+\tau) = \sum_{m=1}^{\infty} \left(\tau \frac{\partial}{\partial t}\right)^m f(t) = \exp\left(\tau \frac{\partial}{\partial t}\right) \frac{f(t)}{m!}.$$

Therefore, Eqs. (B5)–(B6) yield

$$\exp\left(\tau \frac{\partial}{\partial t}\right) \overline{B}_i(t,\boldsymbol{x}) = (\overline{G}_{ij} + \overline{G}_{ij}\overline{\xi}_m \nabla_m + A_{ijm}\nabla_m$$
$$+ C_{ijmn}\nabla_m\nabla_n) \overline{B}_j \equiv \exp(\tau\hat{L}) \, \overline{\boldsymbol{B}},$$
$$(B7)$$

where $\overline{G}_{ij} = \langle\langle G_{ij}\rangle\rangle_{\boldsymbol{w}} = \delta_{ij} + \nabla_j\overline{U}_i \tau + O[(S\tau)^2]$, $\overline{\xi}_i = \langle\langle\hat{\xi}_i\rangle\rangle_{\boldsymbol{w}} = -\overline{U}_i \tau + O[(S\tau)^2]$, $A_{ijm} = \langle\langle\hat{\xi}_m G_{ij}\rangle\rangle_{\boldsymbol{w}}$, $C_{ijmn} = \langle\langle\hat{\xi}_m\hat{\xi}_n G_{ij}\rangle\rangle_{\boldsymbol{w}}$, and we introduced the operator $\hat{L}$, which allows us to reduce the integral equation (B5) to a partial differential equation. Indeed, Eq. (B7), which is rewritten in the form

$$\exp\left[\tau\left(\hat{L} - \frac{\partial}{\partial t}\right)\right] \overline{\boldsymbol{B}} = \overline{\boldsymbol{B}}, \quad (B8)$$

reduces to

$$\frac{\partial \overline{\boldsymbol{B}}}{\partial t} = \hat{L}\overline{\boldsymbol{B}}. \quad (B9)$$

Taylor expansion of the function $\exp(\tau\hat{L})$ reads

$$\exp(\tau\hat{L}) = \hat{E} + \tau\hat{L} + (\tau\hat{L})^2/2 + \cdots, \quad (B10)$$

where $\hat{E}$ is the unit operator. Thus, Eqs. (B7) and (B10) yield

$$\hat{L} \equiv L_{ij} = \frac{1}{\tau}(\overline{G}_{ij} - \delta_{ij} + \overline{\xi}_m \overline{G}_{ij}\nabla_m + A_{ijm}\nabla_m)$$
$$+ D_{ijmn}\nabla_m\nabla_n + O(\nabla^3), \quad (B11)$$

where $D_{ijmn} = (C_{ijmn} - A_{ikm}A_{kjn})/2\tau$. This yields Eq. (30).

APPENDIX C: ORR-KELVIN RANDOM SHEARING WAVES FOR SMALL HYDRODYNAMIC REYNOLDS NUMBERS

We explain here the details that led to the derivation of Eqs. (36) and (37). We seek the solutions of the linearized Eq. (2) for incompressible velocity field $\boldsymbol{u}$ as superpositions of the Orr-Kelvin shearing waves:

$$\boldsymbol{u}(t,\boldsymbol{r}) = \int \boldsymbol{u}(t,\boldsymbol{k}_0) \exp[i\boldsymbol{k}(t) \cdot \boldsymbol{r}] \, d\boldsymbol{k}_0 \quad (C1)$$

(see, e.g., [23,48–50]), where $\boldsymbol{k}_0 = (k_{x0},k_y,k_z)$, $\boldsymbol{k}(t) = (k_{x0} - Sk_y t, k_y, k_z)$, and we neglected the weak Lorentz force. The amplitudes of the shearing waves satisfy the following equations:

$$\frac{\partial u_x(t,\boldsymbol{k}_0)}{\partial t} = \left[2S\frac{k_y k_x(t)}{k^2(t)} - \nu k^2(t) \right] u_x(t,\boldsymbol{k}_0) + f_x, \quad (C2)$$

$$\frac{\partial u_z(t,\boldsymbol{k}_0)}{\partial t} = 2S\frac{k_y k_z}{k^2(t)} u_x(t,\boldsymbol{k}_0) - \nu k^2(t) u_z(t,\boldsymbol{k}_0) + f_z. \quad (C3)$$

These equations were obtained by taking twice the curl of Eq. (2). Equations (C2) and (C3) have explicit solutions:

$$u_x(t,\boldsymbol{k}_0) = \frac{1}{k^2(t)} \int_0^t dt' \, \tilde{G}_\nu(t,t') k^2(t') f_x(t',\boldsymbol{k}_0), \quad (C4)$$

$$u_z(t,\boldsymbol{k}_0) = u_z^{(1)}(t,\boldsymbol{k}_0) + u_z^{(2)}(t,\boldsymbol{k}_0), \quad (C5)$$

$$u_y(t,\boldsymbol{k}_0) = -\frac{1}{k_y} [k_x(t) u_x(t,\boldsymbol{k}_0) + k_z u_z(t,\boldsymbol{k}_0)], \quad (C6)$$

$$u_z^{(1)}(t,\boldsymbol{k}_0) = \int_0^t dt' \, \tilde{G}_\nu(t,t') f_z(t',\boldsymbol{k}_0), \quad (C7)$$

$$u_z^{(2)}(t,\boldsymbol{k}_0) = 2S\,k_y k_z \int_0^t dt' \frac{\tilde{G}_\nu(t,t')}{k^2(t')} u_x(t',\boldsymbol{k}_0), \quad (C8)$$

where $\tilde{G}_\nu(t,t') = \exp[-\nu \int_{t'}^t dt'' k^2(t'')]$. Equations (C4)–(C8) for a white-in-time forcing yield the following formulas for non-instantaneous two-point correlation functions:

$$\langle u_x(t,\boldsymbol{k}_0) u_z^{*(1)}(t',\boldsymbol{k}_0)\rangle = \tilde{G}_\nu(t,t') \frac{k^2(t')}{k^2(t)} \langle u_x(t',\boldsymbol{k}_0) u_z^{*(1)}(t',\boldsymbol{k}_0)\rangle, \quad (C9)$$

$$\langle u_z^{(1)}(t,\boldsymbol{k}_0) u_x^*(t',\boldsymbol{k}_0)\rangle = \tilde{G}_\nu(t,t')\langle u_z^{(1)}(t',\boldsymbol{k}_0) u_x^*(t',\boldsymbol{k}_0)\rangle, \quad (C10)$$

$$\langle u_x(t,\boldsymbol{k}_0) u_z^{*(2)}(t',\boldsymbol{k}_0)\rangle$$
$$= 2S\,k_y k_z \int_0^{t'} dt'' \frac{\tilde{G}_\nu(t',t'')}{k^2(t'')} \langle u_x(t,\boldsymbol{k}_0) u_x^*(t'',\boldsymbol{k}_0)\rangle, \quad (C11)$$

$$\langle u_z^{(2)}(t,\boldsymbol{k}_0) u_x^*(t',\boldsymbol{k}_0)\rangle$$
$$= 2S\,k_y k_z \int_0^t dt'' \frac{\tilde{G}_\nu(t,t'')}{k^2(t'')} \langle u_x(t'',\boldsymbol{k}_0) u_x^*(t',\boldsymbol{k}_0)\rangle, \quad (C12)$$

where for $t'' < t'$

$$\langle u_x(t'',\boldsymbol{k}_0)\, u_x^*(t',\boldsymbol{k}_0)\rangle = \tilde{G}_\nu(t',t'')\,\frac{k^2(t'')}{k^2(t')}\,\langle u_x(t'',\boldsymbol{k}_0)\, u_x^*(t'',\boldsymbol{k}_0)\rangle,$$

(C13)

and for $t'' > t'$

$$\langle u_x(t'',\boldsymbol{k}_0)\, u_x^*(t',\boldsymbol{k}_0)\rangle = \tilde{G}_\nu(t'',t')\,\frac{k^2(t')}{k^2(t'')}\,\langle u_x(t',\boldsymbol{k}_0)\, u_x^*(t',\boldsymbol{k}_0)\rangle.$$

(C14)

[1] H. K. Moffatt, *Magnetic Field Generation in Electrically Conducting Fluids* (Cambridge University Press, New York, 1978).

[2] E. Parker, *Cosmical Magnetic Fields* (Oxford University Press, New York, 1979).

[3] F. Krause and K. H. Rädler, *Mean-Field Magnetohydrodynamics and Dynamo Theory* (Pergamon, Oxford, 1980).

[4] Ya. B. Zeldovich, A. A. Ruzmaikin, and D. D. Sokoloff, *Magnetic Fields in Astrophysics* (Gordon and Breach, New York, 1983).

[5] A. Ruzmaikin, A. M. Shukurov, and D. D. Sokoloff, *Magnetic Fields of Galaxies* (Kluwer Academic, Dordrecht, 1988).

[6] M. Ossendrijver, Astron. Astrophys. Rev. **11**, 287 (2003).

[7] A. Brandenburg and K. Subramanian, Phys. Rep. **417**, 1 (2005).

[8] I. Rogachevskii and N. Kleeorin, Phys. Rev. E **68**, 036301 (2003).

[9] I. Rogachevskii and N. Kleeorin, Phys. Rev. E **70**, 046310 (2004).

[10] T. Elperin, N. Kleeorin, and I. Rogachevskii, Phys. Rev. E **68**, 016311 (2003).

[11] T. Elperin, I. Golubev, N. Kleeorin, and I. Rogachevskii, Phys. Rev. E **76**, 066310 (2007).

[12] A. Brandenburg, Astrophys. J. **625**, 539 (2005).

[13] T. A. Yousef, T. Heinemann, A. A. Schekochihin, N. Kleeorin, I. Rogachevskii, A. B. Iskakov, S. C. Cowley, and J. C. McWilliams, Phys. Rev. Lett. **100**, 184501 (2008).

[14] T. A. Yousef, T. Heinemann, F. Rincon, A. A. Schekochihin, N. Kleeorin, I. Rogachevskii, S. C. Cowley, and J. C. McWilliams, Astron. Nachr. **329**, 737 (2008).

[15] A. Brandenburg, K.-H. Rädler, M. Rheinhardt, and P. J. Käpylä, Astrophys. J. **676**, 740 (2008).

[16] P. J. Käpylä, M. J. Korpi, and A. Brandenburg, Astron. Astrophys. **491**, 353 (2008).

[17] D. W. Hughes and M. R. E. Proctor, Phys. Rev. Lett. **102**, 044501 (2009).

[18] K.-H. Rädler and R. Stepanov, Phys. Rev. E **73**, 056311 (2006).

[19] G. Rüdiger and L. L. Kitchatinov, Astron. Nachr. **327**, 298 (2006).

[20] N. Kleeorin and I. Rogachevskii, Phys. Rev. E **77**, 036307 (2008).

[21] S. Sridhar and K. Subramanian, Phys. Rev. E **79**, 045305(R) (2009).

[22] S. Sridhar and N. K. Singh, J. Fluid Mech. **664**, 265 (2010).

[23] T. Heinemann, A. A. Schekochihin, and J. C. McWilliams, e-print arXiv:0810.2225.

[24] P. J. Käpylä, D. Mitra, and A. Brandenburg, Phys. Rev. E **79**, 016302 (2009).

[25] D. Mitra, P. J. Käpylä, R. Tavakol, and A. Brandenburg, Astron. Astrophys. **495**, 1 (2009).

[26] L. L. Kitchatinov, Astron. Astrophys. **243**, 483 (1991).

[27] K.-H. Rädler, N. Kleeorin, and I. Rogachevskii, Geophys. Astrophys. Fluid Dyn. **97**, 249 (2003).

[28] P. H. Roberts and A. M. Soward, Astron. Nachr. **296**, 49 (1975).

[29] N. Kleeorin and A. Ruzmaikin, Magnetohydrodynamics **2**, 17 (1982).

[30] A. V. Gruzinov and P. H. Diamond, Phys. Rev. Lett. **72**, 1651 (1994).

[31] A. V. Gruzinov and P. H. Diamond, Phys. Plasmas **2**, 1941 (1995).

[32] N. Kleeorin and I. Rogachevskii, Phys. Rev. E **59**, 6724 (1999).

[33] S. A. Orszag, J. Fluid Mech. **41**, 363 (1970).

[34] A. S. Monin and A. M. Yaglom, *Statistical Fluid Mechanics*, Vol. 2 (MIT Press, Cambridge, MA, 1975).

[35] W. D. McComb, *The Physics of Fluid Turbulence* (Clarendon, Oxford, 1990).

[36] A. Pouquet, U. Frisch, and J. Leorat, J. Fluid Mech. **77**, 321 (1976).

[37] N. Kleeorin, I. Rogachevskii, and A. Ruzmaikin, Zh. Eksp. Teor. Fiz. **97**, 1555 (1990) [Sov. Phys. JETP **70**, 878 (1990)].

[38] E. G. Blackman and G. B. Field, Phys. Rev. Lett. **89**, 265007 (2002).

[39] E. G. Blackman and G. B. Field, Phys. Fluids **15**, L73 (2003).

[40] G. B. Field and E. G. Blackman, Astrophys. J. **572**, 685 (2002).

[41] A. Brandenburg, P. Käpylä, and A. Mohammed, Phys. Fluids **16**, 1020 (2004).

[42] A. Brandenburg and K. Subramanian, Astron. Astrophys. **439**, 835 (2005).

[43] A. Brandenburg and K. Subramanian, Astron. Nachr. **328**, 507 (2007).

[44] S. Sur, K. Subramanian, and A. Brandenburg, Mon. Not. R. Astron. Soc. **376**, 1238 (2007).

[45] I. Rogachevskii and N. Kleeorin, Phys. Rev. E **76**, 056307 (2007).

[46] P. Dittrich, S. A. Molchanov, A. A. Ruzmaikin, and D. D. Sokoloff, Astron. Nachr. **305**, 119 (1984).

[47] N. Kleeorin, I. Rogachevskii, and D. Sokoloff, Phys. Rev. E **65**, 036303 (2002).

[48] Kelvin W. Thomson, Philos. Mag. **24**, 188 (1887).

[49] W. M. Orr, Proc. R. Irish Acad. A **27**, 9 (1907).

[50] W. M. Orr, Proc. R. Irish Acad. A **27**, 69 (1907).

[51] I. Rogachevskii and N. Kleeorin, Phys. Rev. E **56**, 417 (1997).

[52] A. Brandenburg, Astrophys. J. **550**, 625 (2001).

[53] N. E. L. Haugen, A. Brandenburg, and W. Dobler, Phys. Rev. E **70**, 016308 (2004).

[54] M. Schrinner, K.-H. Rädler, D. Schmitt, M. Rheinhardt, and U. Christensen, Astron. Nachr. **326**, 245 (2005).

[55] M. Schrinner, K.-H. Rädler, D. Schmitt, M. Rheinhardt, and U. R. Christensen, Geophys. Astrophys. Fluid Dyn. **101**, 81 (2007).

[56] N. Kleeorin and I. Rogachevskii, Phys. Rev. E **67**, 026321 (2003).

[57] M. Ossendrijver, M. Stix, A. Brandenburg, and G. Rüdiger, Astron. Astrophys. **394**, 735 (2002).

[58] P. J. Käpylä, M. J. Korpi, M. Ossendrijver, and M. Stix, Astron. Astrophys. **455**, 401 (2006).

[59] P. J. Käpylä, M. J. Korpi, and I. Tuominen, Astron. Nachr. **327**, 884 (2006).

[60] H. Zhang, D. Sokoloff, I. Rogachevskii, D. Moss, V. Lamburt, K. Kuzanyan, and N. Kleeorin, Mon. Not. R. Astron. Soc. **365**, 276 (2006).